Mon. Not. R. Astron. Soc. **285,** 820–830 (1997)

# Soft X-ray background fluctuations and large-scale structure in the Universe

F. J. Carrera,[1,2] A. C. Fabian[3] and X. Barcons[1]

[1]*Instituto de Física de Cantabria (Consejo Superior de Investigaciones Científicas – Universidad de Cantabria), Avenida de los Castros, 39005 Santander, Spain*
[2]*Mullard Space Science Laboratory, University College London, Holmbury St. Mary, Dorking, Surrey RH5 6NT*
[3]*Institute of Astronomy, Madingley Road, Cambridge CB3 0HA*

Accepted 1996 October 20. Received 1996 October 11; in original form 1996 July 16

## ABSTRACT

We have studied the fluctuations of the soft (0.9–2 keV) X-ray background intensity for $\sim 10$ and $\sim 2$ arcmin beam sizes, using 80 high galactic latitude medium-deep images from the *ROSAT* position sensitive proportional counter (PSPC). These fluctuations are dominated (and well reproduced) by confusion noise produced by sources unresolved with the beam sizes we used. We find no evidence for any excess fluctuations which could be attributed to source clustering. The 95 per cent confidence upper limits on excess fluctuations $\Delta I_{\rm clus}$ are: $(\Delta I_{\rm clus}/I)_{10\,\rm arcmin} \lesssim 0.12$, $(\Delta I_{\rm clus}/I)_{2\,\rm arcmin} \lesssim 0.07$. We have checked the possibility that low surface brightness extended objects (like groups or clusters of galaxies) may have a significant contribution to excess fluctuations, finding that they are not necessary to fit the distribution of fluctuations, and obtaining an upper limit on the surface density for this type of source. Standard cold dark matter models would produce $\Delta I/I$ larger than the above limits for any value of the density of the Universe $\Omega = 0.1 - 1$, unless the bias parameter of the X-ray emitting matter is smaller than unity, or an important fraction of the sources of the soft X-ray background ($\sim 30$ per cent) is at redshifts $z > 1$. Limits on the 2–10 keV excess fluctuations are also considered, showing that X-ray sources in that band have to be at redshifts $z > 1$ unless $\Omega > 0.4$. Finally, if the spatial correlation function of the sources that produce these excess fluctuations is instead a power law, the density contrast $\delta\rho/\rho$ implied by the excess fluctuations reveals that the Universe is smooth and linear on scales of tens of Mpc, while it can be highly non-linear on scales of $\sim 1$ Mpc.

**Key words:** methods: statistical – diffuse radiation – large-scale structure of Universe – X-rays: general.

## 1 INTRODUCTION

Recent optical identification projects using *ROSAT* position sensitive proportional counter (PSPC) observations have resolved an important fraction of the extragalactic X-ray background (XRB) in the $\sim 1$–2 keV band into discrete sources, mostly active galactic nuclei (AGN) and narrow emission line galaxies (NELGs, a mixed bag including Seyfert 2 galaxies, starburst galaxies and galaxies with H II regions) (Boyle et al. 1994, 1995; Jones et al. 1995; Page et al. 1996a).

Below 0.5 keV the fraction of the XRB that is extragalactic is uncertain, with estimates ranging from about 10 to 20 per cent (McCammon & Sanders 1990; Barber & Warwick 1994). The rest has a local origin, probably in a bubble of hot gas surrounding the Sun. Above 2 keV, only $\sim 4$ per cent of the XRB has been resolved. Ongoing identifications of serendipitous sources in *ASCA* images have increased this fraction to about 40 per cent (Inoue et al. 1996).

Whatever the nature of the sources that produce the XRB, and independently of their identification, the inten-

sity of the XRB received from different directions in the sky contains information on the angular distribution and clustering properties of such sources. The study of the distribution of XRB intensities $P(I)$ probes the source flux distribution ($dN/dS$ or number of sources per sky area per unit flux) down to fluxes $S$ below the detection limit (Hasinger et al. 1993; Barcons et al. 1994). This technique is called $P(D)$, $(D=I-\langle I_{\rm XRB}\rangle)$ or fluctuation analysis and is most sensitive to fluxes in which there is about one source per 'beam' (Scheuer 1974; Barcons 1992), the reason being that brighter sources contribute to the bright tail of the (skewed) distribution, while fainter and more numerous sources produce negligibly small noise. However, if the counting noise is important, the technique is only sensitive to source fluxes equivalent to the photon counting noise level.

The effect of source clustering is to decrease the effective number of sources per beam, hence broadening $P(I)$ (Barcons 1992). This broadening can be related to the clustering properties of the sources that produce the XRB, which in turn are the result of density fluctuations in the Universe $\delta\rho/\rho$ (Butcher et al. 1996; Barcons & Fabian 1988; Rees 1980).

Instead of following the usual approach of using the deepest fields available to push our knowledge of $dN/dS$ well below the present detection limits, in this work we have explored the clustering properties of X-ray sources by measuring or limiting the excess fluctuations they produce. Direct deep source counts have been performed over small sky areas, and they might be biased by large-scale fluctuations in the source counts. The use of 80 widely scattered *ROSAT* fields allows a statistical study to be made [through $P(I)$], avoiding any such biases.

The limits obtained on the excess fluctuations are then compared with the specific expectations from a cold dark matter (CDM) model, to constrain the density of the Universe ($\Omega\equiv 2q_0$) and/or the bias parameter of X-ray emitting matter with respect to the underlying matter distribution ($b_{\rm X}$). Assuming instead a power-law shape for the spatial correlation function of the source of the soft XRB, the upper limits obtained on the excess fluctuations have been used to investigate $\delta\rho/\rho$ on different scales.

In Section 2 we describe the data used in this work and the reduction process. A brief summary of $P(I)$ analysis is given in Section 3, along with the $dN/dS$ models used and the results of fitting the theoretical $P(I)$ curves to the data.

Section 4 is devoted to the development of the theoretical framework necessary to relate these excess fluctuations to CDM power spectra and $\delta\rho/\rho$. The limits obtained on $\Omega$ and $b_{\rm X}$ are also presented and discussed, as well as those obtained on $\delta\rho/\rho$. In Section 5 we summarize our results.

We have parametrized the Hubble constant as $H_0=100\,h$ km s$^{-1}$ Mpc$^{-1}$, with $h=0.5$. The X-ray fluxes $S$ will be given by default in the 0.5–2 keV range.

## 2 THE DATA

The data used in this work consist of 80 *ROSAT* PSPC pointings with exposure times longer than 8 ks at Galactic latitudes higher than 20°. These same fields were used for the ROSAT International X-ray Optical Survey (RIXOS) (Mason et al., in preparation). In addition, the RIXOS fields were chosen avoiding extended or very bright targets (e.g. clusters, nearby bright galaxies and bright stars).

The Starlink software package ASTERIX was used for the data reduction. The data were screened for high particle background intervals (Plucinsky et al. 1993), bad aspect ratio solutions, and total accepted count rates deviating from the average of each observation. This procedure normally reduced the nominal exposure time by 10 to 20 per cent. The remaining particle background was then calculated using the formulae in Plucinsky et al. (1993), and subtracted.

The remaining counts in Pulse Height Analyzer (PHA) channels 92 to 201 ($\sim$0.7–2 keV) for each pointing were then binned to obtain images with a pixel size of 4.5 arcsec. These images were then de-vignetted by dividing by the exposure maps provided by the standard EXSAS processing, after normalizing the maps to unity in the centre. We note, however, that the results given below are practically insensitive to whether the remaining particle background is subtracted or not, or whether the vignetting has been corrected for or not.

The range of channels used in this work was chosen to avoid local contributions to the XRB (such as the local bubble and Galactic diffuse emission, both thought to be important only below $\sim$1 keV), solar contamination (usually modelled as an oxygen line at about 0.5 keV, Snowden & Freyberg 1993) and absorption from neutral hydrogen (practically absent above 1 keV). An estimate of the possible solar contamination was obtained by extracting images just using night-time observations (Snowden & Freyberg 1993). This reduced dramatically the total number of counts, hence worsening the statistics, without actually changing significantly the average count rate. We have, therefore, used both day- and night-time data.

A circle of radius 5 arcmin around the target of each of the PSPC fields (generally at the centre) was excluded. This proved sufficient to exclude contributions from the targets down to the level in which their 'tails' would contribute less than 30 per cent of the local background per pixel in the two worst cases. In most of them this contribution was $\lesssim$5 per cent.

Only one of the detected sources in the analysed area in these fields is above the flux interval used in our calculations (see Section 3.1). Excluding that field from our analysis does not affect any of our results, therefore we have used the 80 fields including the detected sources within the regions explained below.

Counts in each of the de-vignetted, particle-background subtracted, target-subtracted images were further grouped into two beam sizes as follows.

(i) An annulus of radii 5 and 10 arcmin centred on the pointing direction (the inner radius is a result of the target subtraction), giving a beam size of $\Omega_{\rm eff}=\pi\times(10^2-5^5)/3600=0.065\,45$ deg$^{-2}$. The distribution, $P(I)$, of the 80 XRB intensities obtained (in counts per second per 'beam'), $I$, is shown in Fig. 1.

(ii) Eight circles of radius 2.5 arcmin with centres equally spaced in a circumference of radius 7.5 arcmin centred on the pointing direction, hence $\Omega^{\rm S}_{\rm eff}=\pi\times(2.5/60)^2=0.005\,45$ deg$^{-2}$. We excluded two of these circular beams because

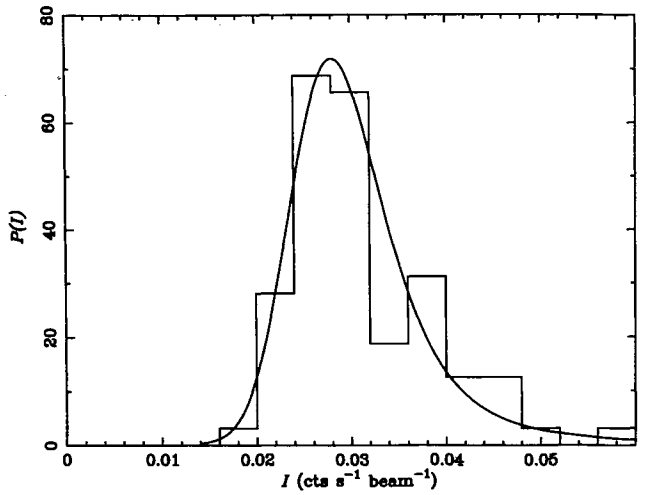


**Figure 1.** Histogram of the distribution of the XRB intensities for the large beam (see text). Also shown as a solid continuous line is the best fit $P(I)$ with $K=55$ deg$^{-2}$, with no cluster contribution and the average $\Delta I_{\rm noise}$ (see text).

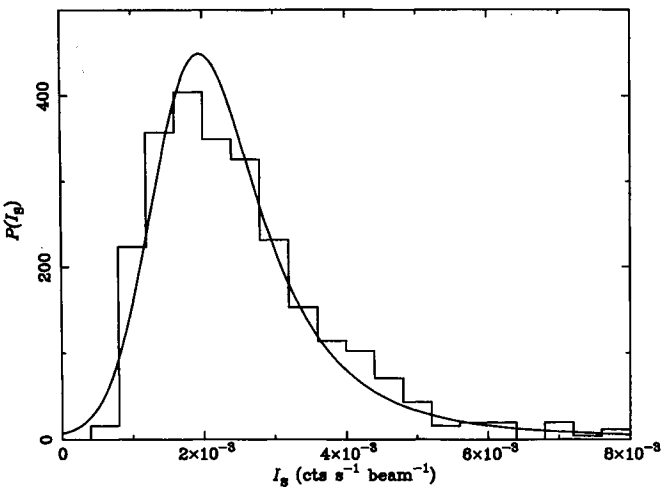


**Figure 2.** Histogram of the distribution of XRB intensities for the small beam (whole data set, see text). Also shown as a solid continuous line is the best fitting $P(I_{\rm S})$ with $K=55$ deg$^{-2}$, with no cluster contribution and the average $\Delta I_{\rm Snoise}$ (see text).

more than one third of their area was taken away by the target exclusion circle (that was slightly off-centre). The remaining 638 values ($80\times 8-2$), $I_{\rm S}$, again in count s$^{-1}$ beam$^{-1}$, give $P(I_{\rm S})$, as shown in Fig. 2.

Both sets of intensities cover similar detector zones, but they sample different angular scales: 10 to 15 arcmin in the first case and $<5$ arcmin in the second. The maximum off-axis angle used (10 arcmin) ensures that the vignetting correction is small ($<5$ per cent) and that the effective area is also uniform over the detector region used.

We found average values of the XRB intensity of $0.49\pm0.02$ count s$^{-1}$ deg$^{-2}$ from the large beam sample and $0.50\pm0.03$ count s$^{-1}$ deg$^{-2}$ from the small beam sample (both $1\sigma$ confidence intervals). We adopt $\langle I_{\rm XRB}\rangle=0.50\pm0.03$ count s$^{-1}$ deg$^{-2}$.

The photon counting noise was estimated by the square root of the number of counts in each 'beam' (using Poisson statistics). We found $\Delta I_{\rm noise}=0.0018\pm0.0005$ count s$^{-1}$ beam$^{-1}$ and $\Delta I_{\rm Snoise}=0.005\pm0.0002$ count s$^{-1}$ beam$^{-1}$; in both cases we give $1\sigma$ confidence intervals.

A conversion factor of 1 count s$^{-1}$ (92–201) $=2.02\times10^{-11}$ erg cm$^{-2}$ s$^{-1}$ (0.5–2 keV) was used throughout, accurate within $\sim5$ per cent for power-law energy spectral indices $\alpha\sim0.4$–$0.7$, hydrogen column densities $N_{\rm H}\sim(0.5$–$20)\times10^{20}$ cm$^{-2}$ and any combination of detector response matrix and effective area, thus covering the observed XRB spectrum (Gendreau et al. 1995; Branduardi-Raymont et al. 1994) and the galactic columns of the *ROSAT* observations used (Mason et al., in preparation).

We therefore measure a total XRB intensity (including sources) of $\langle I_{\rm XRB}\rangle=(3.3\pm0.3)\times10^{-8}$ erg cm$^{-2}$ s$^{-1}$ (0.5–2 keV). This value is somewhat higher than previous XRB intensity estimates, but still overlaps within $\sim2\sigma$ with the value obtained by Branduardi-Raymont et al. (1994), for example.

## 3 FLUCTUATION ANALYSIS

### 3.1 Contribution from point sources

In this work we have adopted the d$N$/d$S$ shape and parameters from Barcons et al. (1994):

$$\frac{{\rm d}N}{{\rm d}S}(S)=\frac{K}{S_{\rm B}}\left(\frac{S}{S_{\rm B}}\right)^{-\gamma_{\rm d}} \quad S<S_{\rm B}$$

$$\frac{{\rm d}N}{{\rm d}S}(S)=\frac{K}{S_{\rm B}}\left(\frac{S}{S_{\rm B}}\right)^{-\gamma_{\rm u}} \quad S>S_{\rm B}$$

with $S_{\rm B}=2.2\times10^{-14}$ erg cm$^{-2}$ s$^{-1}$, $\gamma_{\rm d}=1.8$, $\gamma_{\rm u}=2.5$ and $K=55$ deg$^{-2}$.

The results given below do not change if we use the slightly different parameters from Branduardi-Raymont et al. (1994) or Hasinger et al. (1993), which is hardly surprising considering that they are all mutually consistent, have been obtained with *ROSAT* data and sample similar or overlapping flux ranges. This also means that no biases have been introduced in the determination of the source counts in those surveys by large-scale source number fluctuations.

The d$N$/d$S$ parameters given above are appropriate for $S$ between 0.07 and $50\times10^{-14}$ erg cm$^{-2}$ s$^{-1}$. At the level of one source per beam, the $P(I)$ curve is going to be sensitive down to fluxes $S\sim2\times10^{-14}$ erg cm$^{-2}$ s$^{-1}$ and the $P(I_{\rm S})$ down to $S\sim0.3\times10^{-14}$ erg cm$^{-2}$ s$^{-1}$. The sensitivity limit of our analysis is thus $S\sim10^{-14}$ erg cm$^{-2}$ s$^{-1}$. The width of the $P(I)$ is mainly due to this 'confusion noise' rather than to photon counting noise. Although we are integrating the d$N$/d$S$ between zero and infinity in our calculations, the practicalities of using a fast Fourier transform algorithm to calculate the $P(I)$ effectively reduced this interval to $(0.02$–$40)\times10^{-14}$ erg cm$^{-2}$ s$^{-1}$.

Given a d$N$/d$S$ and a beam profile, the shape of $P(I)$ can be predicted (see Barcons 1992 and references therein). The counting noise is generally taken into account by convolving $P(I)$ with a Gaussian of width $\Delta I_{\rm noise}$. We have also followed this approach, taking as $\Delta I_{\rm noise}$ the average values given above, and checking the influence of the dispersion

around those values by using the $1\sigma$ upper and lower limits as well (see below).

The beam functions are taken as two circular step functions: one with an outer radius of 10 arcmin and an inner radius of 5 arcmin (for $I$), and another with just an outer radius of 2.5 arcmin (for $I_S$). The sizes are much larger than the point spread function (PSF) of the XRT/PSPC combination (Hasinger et al. 1992), making the convolution of the PSF and the step functions indistinguishable from the simple step functions in practice.

Any width in excess of that expected from the source flux distribution and the Poisson counting noise is called excess variance, and is usually modelled by convolving $P(I)$ with a Gaussian of width $\Delta I_{\rm clus}$. We assume that the excess fluctuations arise from clustering of sources, with perhaps some contribution from extended sources like clusters of galaxies (see below). If any other unknown systematic effect contributes to the excess fluctuations, the results given below would just be upper limits to $\Delta I_{\rm clus}$ really arising from clustering, and any consequences of the results given here would be strengthened.

The model $P(I)$ is then (see also equation 22 in Barcons 1992):

$$P(I)=\int {\rm d}\omega e^{-2\pi i\omega I}\exp(-\omega^2\Delta I^2_{\rm noise}/2-\omega^2\Delta I^2_{\rm clus}/2)$$

$$\times\exp\left\{\Omega_{\rm eff}\int {\rm d}S\ {\rm d}N/{\rm d}S\,[\exp(2i\pi\omega S/\Omega_{\rm eff})-1]\right\}. \quad (1)$$

The same expression is valid for $I_S$ replacing $\Omega_{\rm eff}$ with $\Omega^S_{\rm eff}$.

### 3.2 Contribution from extended sources

We have considered the X-ray emitting clusters reported by Rosati et al. (1995). With the above parametrization, a set of parameters that follow their d$N$/d$S$ in the flux range $(1\text{–}40)\times10^{-14}$ erg cm$^{-2}$ s$^{-1}$ is: $\gamma_d=\gamma_u=1.962$, $K_{\rm cl}=9.784$ deg$^{-2}$ and $S_{\rm Bcl}=10^{-14}$ erg cm$^{-2}$ s$^{-1}$.

The properties of these clusters have been taken from the study of poor groups of galaxies by Mulchaey et al. (1996). We have assumed the temperature of the hot gas (responsible for the detected X-ray emission) to be $kT\sim1$ keV and King emission profile with a cluster core size of $R_{\rm core}=15$ arcmin (changing the size to 7 arcmin does not affect the results given below). For a nearby group (like those in Mulchaey et al. 1996) with $z\sim0.02$ this corresponds to a core size of $\sim0.4$ Mpc (or $\sim0.2$ for 7 arcmin).

The conversion factor for clusters, assuming a thermal bremsstrahlung spectrum with the above temperature and absorption by neutral hydrogen with $N_{\rm H}=10^{20}$ cm$^{-2}$, is 1 count s$^{-1}$ (92–201) $=1.64\times10^{-11}$ erg cm$^{-2}$ s$^{-1}$ (0.5–2 keV).

The cluster contribution to $P(I)$ is modelled by convolving it with the $P(I)$ resulting from the clusters only, i.e. by adding another term to the exponent in braces in equation 1,

$$P(I)=\int {\rm d}\omega e^{-2\pi i\omega I}\exp(-\omega^2\Delta I^2_{\rm noise}/2-\omega^2\Delta I^2_{\rm clus}/2)$$

$$\times\exp\left\{\Omega_{\rm eff}\int {\rm d}S\ {\rm d}N/{\rm d}S\,[\exp(2\pi i\omega S/\Omega_{\rm eff})-1]\right\} \quad (2)$$

$$\times\exp\left[2\pi\int dr r\int {\rm d}S\,({\rm d}N/{\rm d}S)_{\rm cl}\{\exp[2\pi i\omega S G_{\rm cl}(r)]-1\}\right]$$

where $G_{\rm cl}(r)$ is the convolution of a King profile with the step functions described above.

Only clusters with fluxes $S>10^{-14}$ erg cm$^{-2}$ s$^{-1}$ (the sensitivity limit of the Rosati et al. sample) have been used to calculate the $P(I)$. Again, the results given below do not change if we decrease this limit by a decade, because of the flatness of the source counts of the clusters.

The angular size of the clusters of galaxies considered here implies that, if one of them is present in a given *ROSAT* pointing, the eight small beams will be affected. This introduces a correlation between them and complicates the error estimates on $\Delta I_{\rm Sclus}$. A way around this problem is to select one of the eight beams for each *ROSAT* pointing at random, and just to use those 80 values of $I_S$. This allows us to estimate the significance of the cluster contribution (at the price of sacrificing sensitivity). Should this contribution prove to be negligible, the whole data set can be used, applying equation (1) instead of equation (2).

### 3.3 Fitting process and results

A maximum likelihood fitting method was adopted. $\chi^2$ was not adequate because the number of fitting points for $P(I)$ was too small to make a significant number of bins with a reasonable number of points in each one of them (enough for Gaussian statistics to be valid).

A further ingredient [apart from d$N$/d$S$, $({\rm d}N/{\rm d}S)_{\rm cl}$, $\Delta I_{\rm noise}$ and $\Delta I_{\rm clus}$] is necessary to fit $P(I)$: the total intensity of the sources in the d$N$/d$S$ used to calculate $P(I)$ ($\langle I\rangle_{{\rm d}N/{\rm d}S}$) is always smaller than the mean observed intensity. The missing sources are *not* important for the shape of $P(I)$, because there are so many of them and they are so faint that they contribute a negligibly small Gaussian noise to it (already taken into account with $\Delta I_{\rm noise}$). Their absence makes the 'peak' of the model $P(I)$ to be at an intensity smaller than that of the peak of the observed distribution, so an overall shift of the distribution is necessary to compare the observed and modelled $P(I)$.

An additional intensity $\Delta I$ is added to each $I$ to shift them to higher values and is allowed to vary until a best fit is obtained (keeping the rest of the parameters fixed). It is then discarded as a non-interesting parameter and the fitting proceeds with a different set of parameters. The best-fitting $\Delta I$ is in fact only very weakly dependent on the rest of the parameters. The value of $\Delta I$ can, however, be predicted from the d$N$/d$S$ and $\langle I_{\rm XRB}\rangle$, and its final best-fitting value is not expected to be very different from this predicted value.

For each set of fitting parameters, we have defined the likelihood function as

$${\rm L}(\Delta I_{\rm clus},K)=-2\sum_i \ln P(I_i)$$

$$+\left(\frac{\langle I_{\rm XRB}\rangle-\Delta I-\langle I\rangle_{{\rm d}N/{\rm d}S}}{\Delta\langle I_{\rm XRB}\rangle}\right)^2, \quad (3)$$

**Table 1.** Results of the fit to $P(I)$.

| $\Delta I_{\rm noise}$ (ct s$^{-1}$ beam$^{-1}$) | $\Delta I_{\rm clus}$ (ct s$^{-1}$ beam$^{-1}$) | $2\sigma$ upper limit (ct s$^{-1}$ beam$^{-1}$) | L | $K$ (deg$^{-2}$) | $K_{\rm cl}$ (deg$^{-2}$) | $2\sigma$ upper limit (deg$^{-2}$) |
|---|---|---|---|---|---|---|
| Mean | 0.0017 | 0.0037 | -556.3 | 55.0 fixed | 9.8 fixed | - |
| Mean+1$\sigma$ | 0.0008 | 0.0034 | -556.3 | " | " | - |
| Mean−1$\sigma$ | 0.0021 | 0.0039 | -556.3 | " | " | - |
| Mean | 0.0006 | 0.0038 | -556.8 | 55.0 fixed | 25.8 | 62.2 |
| Mean+1$\sigma$ | 0.0000 | 0.0035 | -556.6 | " | 19.3 | 55.8 |
| Mean−1$\sigma$ | 0.0013 | 0.0039 | -556.8 | " | 26.0 | 67.2 |
| Mean | 0.0001 | 0.0038 | -557.0 | 67.3 | 9.8 fixed | - |
| Mean+1$\sigma$ | 0.0000 | 0.0037 | -556.7 | 61.9 | " | - |
| Mean−1$\sigma$ | 0.0003 | 0.0040 | -557.1 | 71.1 | " | - |
| Mean | 0.0022 | 0.0041 | -555.6 | 55.0 fixed | 0.0 fixed | - |
| Mean+1$\sigma$ | 0.0016 | 0.0038 | -555.6 | " | " | - |
| Mean−1$\sigma$ | 0.0025 | 0.0043 | -555.6 | " | " | - |
| Mean | 0.0001 | 0.0038 | -557.1 | 74.1 | 0.0 fixed | - |
| Mean+1$\sigma$ | 0.0003 | 0.0037 | -556.5 | 62.9 | " | - |
| Mean−1$\sigma$ | 0.0001 | 0.0039 | -557.2 | 78.3 | " | - |

**Table 2.** Results of the fit to $P(I_{\rm S})$.

| $N$ | $\Delta I_{\rm Snoise}$ (ct s$^{-1}$ beam$^{-1}$) | $\Delta I_{\rm Sclus}$ (ct s$^{-1}$ beam$^{-1}$) | $2\sigma$ upper limit (ct s$^{-1}$ beam$^{-1}$) | L | $K$ (deg$^{-2}$) | $K_{\rm cl}$ (deg$^{-2}$) | $2\sigma$ upper limit (deg$^{-2}$) |
|---|---|---|---|---|---|---|---|
| 80 | Mean | 0.0000 | 0.0004 | -861.7 | 55.0 fixed | 9.8 fixed | - |
| " | Mean+1$\sigma$ | 0.0000 | 0.0004 | -857.5 | " | " | - |
| " | Mean-1$\sigma$ | 0.0003 | 0.0005 | -861.9 | " | " | - |
| 80 | Mean | 0.0000 | 0.0004 | -862.1 | 55.0 fixed | 0.0 | 49.6 |
| " | Mean+1$\sigma$ | 0.0000 | 0.0004 | -858.6 | " | 0.0 | 31.9 |
| " | Mean-1$\sigma$ | 0.0003 | 0.0006 | -862.2 | " | 0.0 | 83.9 |
| 80 | Mean | 0.0000 | 0.0007 | -862.0 | 49.5 | 9.8 fixed | - |
| " | Mean+1$\sigma$ | 0.0000 | 0.0006 | -861.8 | 31.0 | " | - |
| " | Mean-1$\sigma$ | 0.0003 | 0.0008 | -861.9 | 55.0 | " | - |
| 80 | Mean | 0.0000 | 0.0004 | -862.1 | 55.0 fixed | 0.0 fixed | - |
| " | Mean+1$\sigma$ | 0.0000 | 0.0004 | -858.6 | " | " | - |
| " | Mean-1$\sigma$ | 0.0003 | 0.0006 | -862.2 | " | " | - |
| 80 | Mean | 0.0000 | 0.0007 | -862.2 | 52.5 | 0.0 fixed | - |
| " | Mean+1$\sigma$ | 0.0000 | 0.0006 | -862.0 | 34.1 | " | - |
| " | Mean-1$\sigma$ | 0.0003 | 0.0008 | -862.2 | 55.0 | " | - |
| 638 | Mean | 0.0000 | 0.0002 | -6820 | 55.0 fixed | 0.0 fixed | - |
| " | Mean+1$\sigma$ | 0.0000 | 0.0002 | -6797 | " | " | - |
| " | Mean-1$\sigma$ | 0.0003 | 0.0004 | -6820 | " | " | - |
| 638 | Mean | 0.0000 | 0.0002 | -6823 | 62.6 | 0.0 fixed | - |
| " | Mean+1$\sigma$ | 0.0000 | 0.0002 | -6800 | 47.3 | " | - |
| " | Mean-1$\sigma$ | 0.0000 | 0.0002 | -6836 | 76.5 | " | - |

where the first term is the usual definition [and $P(I)$ is as defined in equation 1 or 2], and the second term makes added intensities far from their expected values less likely, weighted for each beam size with the error in the estimate of the XRB intensity, $\Delta\langle I_{\rm XRB}\rangle$, given above. With this definition $\Delta$L is distributed as $\Delta\chi^2$.

The first fit is performed fixing all the d$N$/d$S$ parameters to the values given above and leaving $\Delta I_{\rm clus}$ as the only free parameter. The best-fitting values are shown in Table 1 (for the large beam) and Table 2 (for the small beam). The effect of the uncertainty on $\Delta I_{\rm noise}$ has been assessed by fixing it to its mean value and the $1\sigma$ upper and lower limits, and performing the fit for each of these three values. The results are indicated in Tables 1 and 2 (rows with both the $K$ and $K_{\rm cl}$ columns labelled 'fixed'), with the first row of each group of three corresponding to the mean, and the second and the third line to the $1\sigma$ upper limit and lower limit, respectively. At the $2\sigma$ confidence level, only upper limits are obtained: $\Delta I_{\rm clus} < 0.004$ count s$^{-1}$ beam$^{-1}$ and $\Delta I_{\rm Sclus} < 0.0005$ count s$^{-1}$ beam$^{-1}$ (or $\Delta I_{\rm clus}/\langle I_{\rm XRB}\rangle < 12$ per cent and $\Delta I_{\rm Sclus}/\langle I_{\rm XRB}\rangle < 19$ per cent).

The d$N$/d$S$ normalization, $K$, and $\Delta I_{\rm clus}$ are coupled to some extent: large normalizations increase the 'intrinsic' $P(I)$ width, thus reducing the amount of excess variance needed. We have done a second set of fits in two dimensions, with both $K$ and $\Delta I_{\rm clus}$ as free parameters. The results

are shown in Tables 1 and 2. ΔL contours are plotted in Figs 3 (large beam) and 4 (small beam), for the case of no cluster contribution (and the whole data set, see below) and the average values of $\Delta I_{\rm noise}$ and $\Delta I_{\rm Snoise}$, respectively.

It is possible to obtain confidence intervals on $\Delta I_{\rm clus}$ taking into account its coupling with $K$ by finding the minimum ΔL value as a function of $K$ for every $\Delta I_{\rm clus}$, and then considering them as a one dimensional ΔL profile for $\Delta I_{\rm clus}$ (Lampton, Margon & Bowyer 1976). This has been done for the results plotted in Figs 3 and 4, and it is shown in Figs 5 and 6, respectively, as well as in Tables 1 and 2. As in the one dimensional case, at the $2\sigma$ confidence level, only upper limits are obtained: $\Delta I_{\rm clus} < 0.004$ count s$^{-1}$ beam$^{-1}$ and $\Delta I_{\rm Sclus} < 0.0006 - 0.0008$ count s$^{-1}$ beam$^{-1}$ (or $\Delta I_{\rm clus}/\langle I_{\rm XRB}\rangle < 12$ per cent and $\Delta I_{\rm Sclus}/\langle I_{\rm XRB}\rangle < 22$–30 per cent).

All the above fits have been repeated without any cluster contribution, and the results also included in Tables 1 and 2. It is clear that adding the clusters does not significantly reduce the L values, nor does it reduce the excess variance. We obtained a quantitative assessment of the significance of this contribution using the standard F-test (Bevington 1969). This assesses the relative improvement in $\chi^2$ (or L) on the addition of a new free fitting parameter ($K_{\rm cl}$); in our case that means comparing the values of L in the second and fourth groups of rows in Tables 1 and 2. The F-test reveals that the addition of $K_{\rm cl}$ does not significantly improve the fits, to a confidence of 96 per cent for the large beam, and that the best fit for the small beam actually corresponds to $K_{\rm cl} = 0$. We can then conclude that their contribution to the $P(I)$ width is negligible and ignore it. This allows us to use the full 638 values of $I_{\rm S}$, reducing considerably the $2\sigma$ upper limit in the excess variance: $\Delta I_{\rm Sclus} < 0.0002$ count s$^{-1}$ beam$^{-1}$ (or $\Delta I_{\rm Sclus}/\langle I_{\rm XRB}\rangle < 7$ per cent).

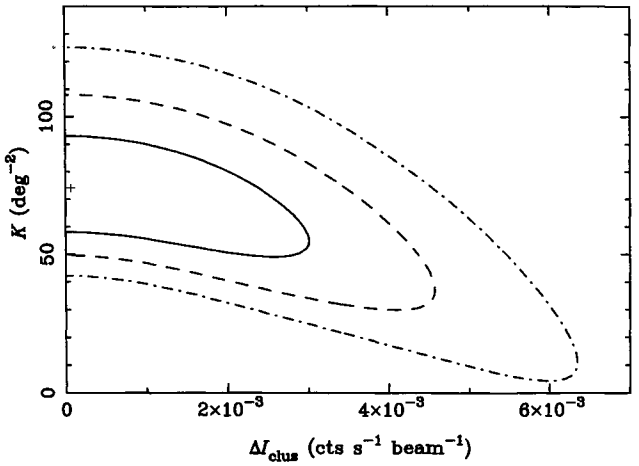


**Figure 3.** Contours of ΔL values (1, 2 and $3\sigma$) in ($K$, $\Delta I_{\rm clus}$) space, for the large beam, with no cluster contribution and the mean $\Delta I_{\rm noise}$ (see text).

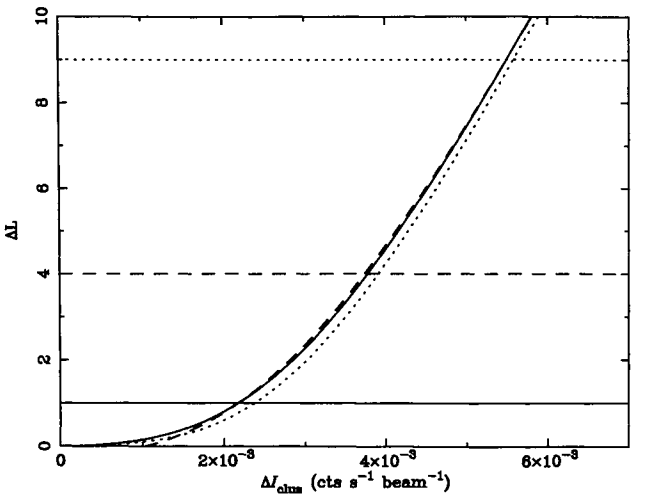


**Figure 5.** One-dimensional ΔL profiles extracted from the contours in Fig. 3 (see text) as a function of $\Delta I_{\rm clus}$. The solid line corresponds to the mean $\Delta I_{\rm noise}$, and the dashed and dotted lines correspond to adding and subtracting $1\sigma$ from it, respectively.

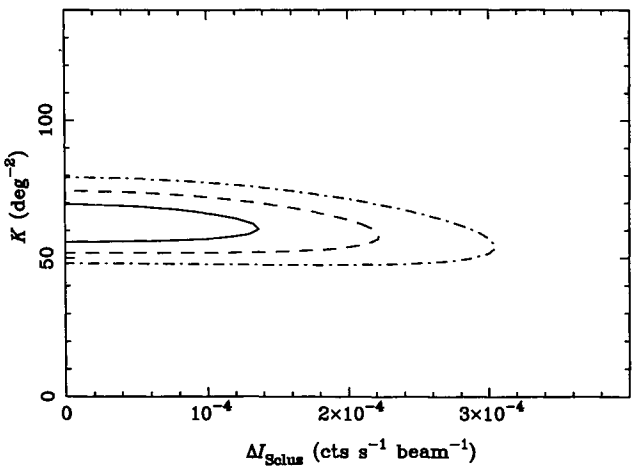


**Figure 4.** Contours of ΔL values (1, 2 and $3\sigma$) in ($K$, $\Delta I_{\rm Sclus}$) space, for the small beam, with no cluster contribution and the mean $\Delta I_{\rm Snoise}$ and the whole data set (see text).

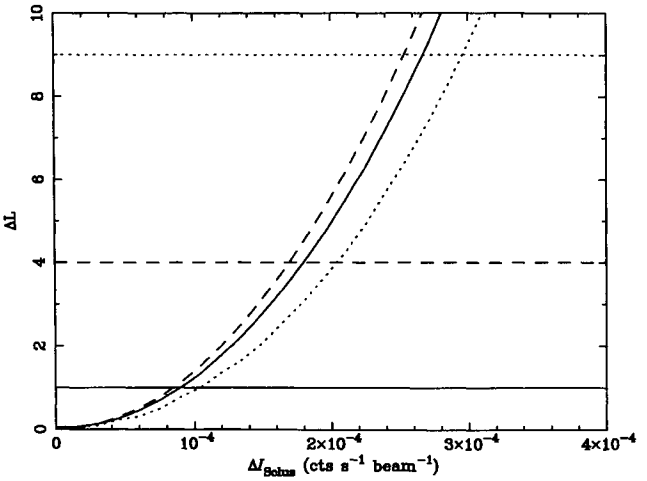


**Figure 6.** One-dimensional ΔL profiles extracted from the contours in Fig. 4 (see text) as a function of $\Delta I_{\rm Sclus}$. The solid line corresponds to the mean $\Delta I_{\rm Snoise}$, and the dashed and dotted lines correspond to adding and subtracting $1\sigma$ from it, respectively.

Confidence regions on $K_{cl}$ can be obtained from the $\Delta L$ contours in the $(\Delta I_{clus}, K_{cl})$ space with the method described above. Only upper limits are obtained at the $2\sigma$ level, and are given in Tables 1 and 2. Rosati et al. warn that their value is only a lower limit to the real surface density of clusters (or extended X-ray sources). Our results show that down to $10^{-15}$–$10^{-14}$ erg cm$^{-2}$ s$^{-1}$, the surface density of clusters is not larger than 3 to 6 times the value obtained by Rosati et al.

Sołtan et al. (1996) found an important contribution ($\sim$30 per cent) to the angular correlation function of the soft XRB from extended haloes around Abell clusters of galaxies on scales $>1$ degree. Since we are exploring much smaller angular scales and the opposite (low flux) end of the $dN/dS$ distribution of the X-ray emitting clusters, there is no contradiction between our finding that extended sources (clusters) do not contribute significantly to the excess fluctuations and the results of Sołtan et al. (1996).

The upper limits on the excess fluctuations obtained in this section (namely, $\Delta I_{clus} < 12$ per cent and $\Delta I_{Sclus} < 7$ per cent, with a $2\sigma$ confidence level), will be used in Section 5 to constrain the values of the density parameter of $\Omega$ and $b_X$ using the expressions derived in Section 4.

## 4 INHOMOGENEITIES IN THE MASS DISTRIBUTION OF THE UNIVERSE

### 4.1 Relation of excess fluctuations to the power spectrum

It is easy to realize that $(\Delta I_{clus}/\langle I_{XRB}\rangle)^2$ is the value of the autocorrelation function of the XRB at zero-lag. We can then use the expressions in Appendix A of Barcons & Fabian (1988) and equations (2) and (4) of Carrera et al. (1991) to relate the limits found on the excess fluctuations to the clustering properties of the sources of the XRB.

In our case, the beam shape is a two-sided step function, with a value of 1 between $r_1$ and $r_2$ and 0 outside, where $r_1 = 5$ arcmin and $r_2 = 10$ arcmin for the large beam, and $r_1 = 0$ and $r_2 = 2.5$ arcmin for the small beam. Its two-dimensional Fourier transform is

$$\hat{G}(q) = [r_2 J_1(r_2 q) - r_1 J_1(r_1 q)]/q, \qquad (4)$$

where $q$ is the magnitude of the two-dimensional Fourier space vector, and $J_1(x)$ is the Bessel function of order 1.

Solving equations (2) and (4) in Carrera et al. (1991) for $\langle I_{XRB}\rangle$, we arrive at

$$\frac{1}{f^2}\left(\frac{\Delta I_{clus}}{\langle I_{XRB}\rangle}\right)^2 = \frac{1}{4\sqrt{2\pi}} \times \frac{c}{H_0}\int dz\,(1+z)^{-8}(1+2q_0 z)^{-1/2} j^2(z)/d_A^2(z) \times \int d^2q\,\hat{G}^2(q)\,\hat{\xi}[q/d_A(z)] \times \left[\frac{\Omega_{eff}}{4\pi}\frac{c}{H_0}\int dz\,(1+z)^{-5}(1+2q_0 z)^{-1/2} j(z)\right]^{-2}, \qquad (5)$$

$d_A(z)$ being the angular distance and $j(z)$ the K-corrected volume emissivity (emitted power per unit volume) of the sources that produce the excess variance and contribute a fraction $f$ to the XRB. $\hat{\xi}(k)$ is the three-dimensional Fourier transform of the spatial correlation function $\xi(r)$, and $k$ is the magnitude of the three-dimensional Fourier space vector. Following Peebles (1980), $\hat{\xi}(k)$ is also the power spectrum, multiplied by $(2/\pi)^{3/2}$, due to the different definitions of the Fourier transform used here and in Peebles (1980).

Equation (5) allows the calculation of $\Delta I_{clus}/\langle I_{XRB}\rangle$ for a particular $b_X$ and a power spectrum model, which in turn would depend on $\Omega$ (see below). By comparing these predictions with the upper limits obtained above, constraints can be placed on those cosmological parameters. In the next section we present the luminosity function we have used to calculate $j(z)$.

### 4.2 Luminosity functions and modelling

At the flux levels at which our $P(I)$ analysis is sensitive ($S \sim 10^{-14}$ erg cm$^{-2}$ s$^{-1}$), the dominant types of X-ray sources found in *ROSAT* surveys are AGN, although with an increasingly important fraction of NELGs (McHardy et al., in preparation; Mason et al., in preparation; Boyle et al. 1994; Boyle et al. 1995; Carballo et al. 1995).

The X-ray luminosity function (XLF, number of sources per unit volume and unit luminosity) of AGN has been very well studied recently with *ROSAT* at those fluxes (Boyle et al. 1994; Page et al. 1996a). It has been found to be well represented by a broken power law. Within a pure luminosity evolution model, the AGN luminosities have a fast positive evolution up to $z \sim 1.5$–$2$. At that redshift the evolution slows down, or even stops and becomes negative.

We have obtained the emissivity $j(z)$ in equation (5) by integrating the best-fitting XLF models of Page et al. (1996a), since AGN are the main contributors to the XRB over the flux range studied. Indeed, AGN are $\sim$50 per cent of the sources at the fluxes we are dealing with, and we have to consider the redshift evolution of the volume emissivity from other sources. The evolution of NELGs, the other type of source with a sizeable contribution and likely to be clustered, is somewhat different (Page et al. 1996b; Boyle et al. 1995). Their rate of evolution is lower than that of AGN, and they are concentrated at low $z$ ($<0.6$).

We have adopted the best power-law model with cut-off evolution and $q_0 = 0.5$ with a conversion factor of 1.8 (between *ROSAT* and *Einstein* fluxes) from Page et al. (1996a), but making $q_0$ half the value of $\Omega$ investigated in each case. The other best-fitting models produce very similar $\Delta I_{clus}/\langle I_{XRB}\rangle$ values. The K-correction has been calculated using $\alpha \sim 1$, as observed for AGN, the dominant type of sources in our flux range (Mittaz et al., in preparation; Almaini et al. 1996; Ciliegi et al. 1996; Romero-Colmenero et al. 1996; Vikhlinin et al. 1995).

We have also considered the results on 2–10 keV *Ginga* excess fluctuations from Butcher et al. (1996): $(\Delta I_{clus}/\langle I_{XRB}\rangle) < 0.038$ ($2\sigma$). In this case the redshift dependence of the emissivity $j(z)$ of the sources is not known and we have adopted a very simple model for their redshift distribution: $j(z) \propto (1+z)^{3+p}$. $p=0$ corresponds to no evolution of the emissivity in comoving coordinates. For a simple power-law luminosity function, $p \sim 3$ implies a luminosity evolution

similar to that found in the soft band. We have approximated the *Ginga* collimator shape by a Gaussian of dispersion $\gamma_S \sim 0.8$ deg, and used an energy index of $\alpha = 0.7$ as observed for AGN in that band.

Making $f = 1$ in equation (5) is equivalent to assuming that the sources whose clustering produces the excess fluctuations we are studying produce all the XRB. We know that only 50–60 per cent of the XRB is produced by sources with fluxes larger than $\sim 10^{-14}$ erg cm$^{-2}$ s$^{-1}$ (our sensitivity limit). However, since in equation (5) the absolute normalization of the XLF cancels out, just having more sources with the same evolution would not affect our theoretical $\Delta I/I$ (this would be the case if NELGs evolved as AGN). We have also checked that extending the integrals in redshift in equation (5) to $z = 5$ instead of $z = 3$ (our default value) does not affect our results. If, as discussed above, the NELGs are proved to make an important contribution to the XRB, but with a different evolution (more concentrated at lower $z$), the resulting density fluctuations produced by these sources would be larger, hence *strengthening* our results.

A similar argument can be used for the *Ginga* upper limits.

### 4.3 CDM models

CDM models present a picture of the Universe in which the smallest structures (galaxies) form first and, by merging, form larger structures (Peacock & Dodds 1994). Even if the basic assumptions have not been thoroughly tested, the CDM scenario provides useful calculation tools and expressions to analyse the evolution of the Universe.

This is the case for the power spectrum of density fluctuations $P(k)$. A number of useful parametrizations that fit some of the available angular and spatial clustering data are found in the literature (Peacock & Dodds 1994, hereafter PD; Efstathiou, Bond & White 1992, hereafter EBW; Bardeen et al. 1986).

We have used the shape of the *linear* power spectrum of PD,

$$P(k) \propto \frac{k^4}{4\pi k^3} \left\{ \frac{\ln(1+gk)}{gk} \right\}^2 \times \{[1 + ak + (bk)^2 + (ck)^3 + (dk)^4]^{-1/4}\}^2, \quad (6)$$

where $a = (3.89/\Gamma)\, h^{-1}$ Mpc, $b = (14.1/\Gamma)\, h^{-1}$ Mpc, $c = (5.46/\Gamma)\, h^{-1}$ Mpc, $d = (6.71/\Gamma)\, h^{-1}$ Mpc, $g = (2.34/\Gamma)\, h^{-1}$ Mpc, and $\Gamma$ is a shape parameter that can be changed, both to make equation (6) fit several different observations, and to reflect the behaviour of different CDM and mixed dark matter models. Following PD, we have chosen

$$\Gamma = \Omega h \exp(-2\Omega_B), \quad (7)$$

which is equivalent to that presented by EBW for zero baryonic density $\Omega_B = 0$, but also includes an empirical dependence in $\Omega_B$, making high baryonic content models mimic low CDM density. The power spectrum parametrization with the shapes and parameters from EBW is similar (for a power spectrum index $n = 1$).

PD also give a dependency of the normalization of $P(k)$ with $\Omega$: $\sigma_8 = 0.75\Omega^{-0.15}$, $\sigma_8$ being the root mean square (rms) density contrast when averaged over spheres of radius $8\, h^{-1}$ Mpc. We have adopted this normalization dependence on $\Omega$. For each value of $\Omega$ we have calculated $\sigma_8$ from equation (6), rescaling its normalization to give the value of $\sigma_8(\Omega)$ given above. This normalized $P(k)$ is then used to calculate $\Delta I/I$.

Standard primordial nucleosynthesis and abundances observations constrain $\Omega_B \sim 0.05$ (Olive & Steigman 1995), and we have assumed this value. Since $\Omega_B$ only appears in an exponent and is small in any case, changing it by $\pm 0.01$ (its observational confidence interval) does not change the results given below.

X-ray sources are possibly more clustered than the underlying matter, and therefore the $\Delta I_{clus}/\langle I_{XRB}\rangle$ obtained from CDM has to be multiplied by the bias parameter $b_X$. A value $b_X \sim (3.4 \pm 0.8)\Omega^{0.6}/f'$ has been found for nearby bright X-ray sources, where $f'$ is the fraction of the gravitational acceleration on the Local Group contributed by the $z < 0.015$ region ($f' \sim 0.5$, Miyaji 1994).

With all the above assumptions, our CDM $\Delta I_{clus}/\langle I_{XRB}\rangle$ only has two free parameters: $\Omega$ and $b_X$. We have sampled $\Omega$ between 0.1 and 1, and assumed $b_X = 1$. Different values of $\Omega$ change the shape of the CDM power spectrum (through the shape parameter $\Gamma$), while the effect of $b_X$ is just multiplicative.

The above CDM power spectrum shape is constant in comoving coordinates. Its evolution with redshift is obtained by multiplying its normalization by a factor $D^2(z)$ that is proportional to $(1+z)^{-2}$ for $\Omega = 1$, and has a more complicated dependence with redshift for smaller values of $\Omega$ (Peebles 1980).

We present in Table 3 $\Delta I_{clus}/\langle I_{XRB}\rangle$ obtained for the beam sizes and shapes used here (small and large beam), for several different values of $\Omega$ in the above range, $b_X = 1$ and the PD power spectrum given in equation (6) (the power spectrum of EBW produces similar results). $\Delta I/I$ produced by CDM exceeds our small beam upper limits ($\Delta I_{Sclus}/\langle I_{XRB}\rangle < 0.07$), for any value of $\Omega$. The power spectrum of the spatial distribution of the X-ray emitting matter is not compatible with CDM.

We have also used the non-linear scaling of the power spectrum proposed by PD. This only increases the excess fluctuations from CDM (by about 50 per cent for the small beam, the more stringent limit), hence worsening the mismatch. A faster clustering evolution does not therefore help reconcile CDM with the upper limits of the excess fluctuations.

If either $b_X < 1$ (i.e. the X-ray sources are *less* clustered than the underlying mass distribution) or $f < 1$ (i.e. the

**Table 3.** $\Delta I_{clus}/\langle I_{XRB}\rangle$ from cold dark matter for *ROSAT*. Linear power spectrum from Peacock & Dodds (1994).

| $\Omega$ | $\frac{\Delta I_{Sclus}}{\langle I_{XRB}\rangle}$ | $\frac{\Delta I_{clus}}{\langle I_{XRB}\rangle}$ |
|---|---|---|
| 0.1 | 0.107 | 0.098 |
| 0.2 | 0.098 | 0.086 |
| 0.4 | 0.097 | 0.081 |
| 0.6 | 0.101 | 0.080 |
| 0.8 | 0.106 | 0.081 |
| 1.0 | 0.111 | 0.083 |
| Upper limits | 0.072 | 0.119 |

sources considered in our XLF do not produce the whole of the XRB), CDM models would be consistent with the upper limits of our excess fluctuations, provided that $f \times b_X \lesssim 0.7$.

We have already shown that the X-ray sources more clearly associated with peaks on the matter distribution (clusters) are not relevant for the excess fluctuations. However, AGN and NELGs have been shown to be important contributors to the soft X-ray background (50 to 60 per cent of it has been resolved into these types of sources), and both populations seem to cluster in the same comoving scales as 'normal' galaxies do (see Boyle & Mo 1993 for a study of the clustering of X-ray AGN, and Shanks & Boyle 1994). Values of $b_X$ between 1 and 8 would be obtained from the results of Miyaji (1994), with $\Omega$ varying in the above range. A value of the bias parameter $b_X < 1$ is therefore very unlikely.

As discussed at the end of Section 4.2, the absolute normalization of the emissivity of the sources that produce the excess fluctuations $j(z)$ cancels out. We also commented that, if an important fraction of those sources were distributed at smaller redshifts than the population considered in the XLF used here, the calculated excess fluctuations produced would *increase*. About 95 per cent of the excess fluctuations from CDM are produced at $z < 1$; sources at higher redshift do not contribute significantly to the excess fluctuations. From this it follows that one possible way of getting $f \sim 0.7$ to reconcile CDM and XRB fluctuations would be to place the unresolved part of the sources of the XRB at $z > 1$.

$\Delta I_{clus}/\langle I_{XRB}\rangle$ calculated for a *Ginga* beam size and a power-law emissivity evolution are given in Table 4 for $p = 0$, 3 and two different values of the maximum redshift of integration $z_{max} = 1$, 3. The minimum redshift was set at 0.05; changing it to 0.1 did not change the results significantly. For a comoving evolution $p = 0$, the upper limits are exceeded at all values of $\Omega$, and the maximum fraction contributed by $z < 1$ sources is $f < 0.3$. A positive evolution is in principle more plausible, in line with the soft XLF results quoted above. For $p = 3$, about 50 per cent of the XRB intensity has to come from $z > 1$ to reconcile the upper limits with the CDM excess fluctuations. Alternatively, most (70–90 per cent) of the XRB sources could be nearby, but then the density of the Universe cannot be low ($\Omega > 0.2$–$0.4$).

**Table 4.** $\Delta I_{clus}/\langle I_{XRB}\rangle$ from cold dark matter for *Ginga*. Linear power spectrum from Peacock & Dodds (1994).

| | $p = 0$ | | $p = 3$ | |
|---|---|---|---|---|
| $z_{max}$ | 1 | 3 | 1 | 3 |
| $\Omega$ | $\Delta I_{clus}/\langle I_{XRB}\rangle$ | | | |
| 0.1 | 0.219 | 0.222 | 0.066 | 0.113 |
| 0.2 | 0.174 | 0.176 | 0.051 | 0.081 |
| 0.4 | 0.142 | 0.143 | 0.040 | 0.059 |
| 0.6 | 0.129 | 0.129 | 0.036 | 0.050 |
| 0.8 | 0.121 | 0.122 | 0.033 | 0.045 |
| 1.0 | 0.116 | 0.117 | 0.032 | 0.043 |
| Upper limit | 0.038 | 0.038 | 0.038 | 0.038 |

Similar upper limits on $f$ were obtained from studies of the angular correlation function of the XRB both above and below 2 keV and in angular scales between 1 arcmin and several degrees (see e.g. Carrera et al. 1991; Sołtan & Hasinger 1994). However, the alternative possibility in those studies of a rapid evolution of the source clustering would not be consistent with our data, as discussed above.

### 4.4 Limits on the density contrast from excess fluctuations

In this section, we will investigate the density contrast of matter in the Universe ($\delta\rho/\rho$) implied by the upper limits obtained on the excess fluctuations. Instead of using a CDM power spectrum, we assume that the sources of the XRB have a spatial correlation function $\xi(r) = (r/r_0)^{-1.8}$ with a comoving evolution. By performing its Fourier transform and substituting in equation (5), we can translate the limits on $\Delta I_{clus}/\langle I_{XRB}\rangle$ to limits on the spatial correlation length $r_0$.

The density contrast $\delta\rho/\rho$ in a window $W(\boldsymbol{r})$ is given by

$$(\delta\rho/\rho)^2 = \int \mathrm{d}^3\boldsymbol{k}\,\hat{\xi}(\boldsymbol{k})\,\hat{W}^2(\boldsymbol{k}) \qquad (8)$$

where $\hat{W}(\boldsymbol{k})$ is the Fourier transform of the window function, that we have taken here to be a sphere of radius $R$. For this window function and a power-law correlation function, $\delta\rho/\rho$ is also a power law on $R$: $(\delta\rho/\rho)^2 \propto (r_0/R)^{1.8}$. We can therefore use the limits on $r_0$ obtained from equation (5) (with the emissivities discussed in Section 4.2) to constrain $\delta\rho/\rho$. The resulting upper limits on $\delta\rho/\rho$ versus $R$ are plotted in Fig. 7, using both our limits on the excess fluctuations from *ROSAT*, and Butcher et al.'s (1996) results from *Ginga* (assuming $p = 3$ that gives the more conservative upper limits). We have used $\Omega = 0.1$ in Fig. 7. If instead we use $\Omega = 1$, the limits are 10–20 per cent smaller.

Given the size of the different beams used, this analysis is going to be sensitive to different sampling radii. We have estimated the relevant ranges by using a typical angular

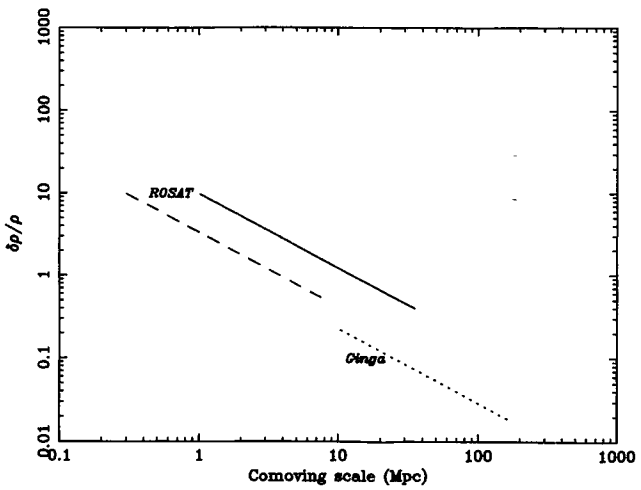


**Figure 7.** $\delta\rho/\rho$ limits at different scales (see text): the solid line is the *ROSAT* upper limit from the large beam, the dashed line is the small beam upper limit, the dotted line is the *Ginga* upper limit.

distance for each beam size involved ($\sim$3 arcmin for our *ROSAT* small beam, $\sim$12 arcmin for our large beam, and $\sim 1°$ for *Ginga*) and calculating the maximum and minimum separations it corresponds to for the redshift range considered ($z \sim 0.05$–3 for *ROSAT*, and $z \sim 0.1$–3 for *Ginga*). As we can see in Fig. 7, the smaller angular scale results are sensitive to spatial distances of the order of 1 Mpc, while the larger ones are sensitive to a few tens of Mpc.

At the larger scale sampled here the Universe is quite homogeneous ($\delta\rho/\rho < 1$), while below a few Mpc there is space for strong density fluctuations ($\delta\rho/\rho > 1$) that would reveal a highly non-linear growth of structure.

## 5 SUMMARY

Our fluctuation analysis of 80 *ROSAT* fields has allowed us to constrain the excess fluctuations on $\sim$10 arcmin angular scales to be $\Delta I_{\rm clus} < 0.004$ count s$^{-1}$ beam$^{-1}$ and on $\sim$2 arcmin $\Delta I_{\rm Sclus} < 0.0002$ count s$^{-1}$ beam$^{-1}$ (or $\Delta I_{\rm clus}/\langle I_{\rm XRB}\rangle < 17$ per cent and $\Delta I_{\rm Sclus}/\langle I_{\rm XRB}\rangle < 7$ per cent), both with $2\sigma$ confidence levels.

The source counts found in medium and deep surveys in empty fields reproduce well the fluctuations of the XRB around bright targets (most of which are nearby galaxies of different types). Since there is no need for any excess fluctuation, we conclude that faint X-ray sources are not associated with local astronomical objects.

A contribution from extended objects with low surface brightness (like groups or clusters of galaxies) is not required to fit the observed distribution of intensities. The surface density of these objects is shown to be $<$3–6 times the observed value, limiting the fraction of low surface brightness sources missed by present surveys.

The upper limits on $\Delta I_{\rm clus}/\langle I_{\rm XRB}\rangle$ obtained here (and others from the literature) have been compared with CDM theoretical models to extract constraints on the density parameter of the Universe $\Omega$ and the bias parameter of X-ray emitting sources with respect to the underlying matter distribution $b_{\rm X}$. Unless $b_{\rm X} \sim 0.7$ (which is unlikely), the only possibility for reconciling our results with CDM would be that the remaining unresolved sources of the soft XRB (contributing 30 per cent of it) are at $z > 1$, and have suffered a cosmological evolution different from the other known sources of the soft XRB (AGN and NELGs). Similarly, sources that produce about 50 per cent of the 2–10 keV XRB have to be at $z > 1$; this fraction could be larger if $\Omega > 0.4$.

In a different approach, a power-law shape is assumed instead for the spatial correlation function of the XRB sources, constraining the density contrast to be $<1$ on scales of tens of Mpc and $<10$ around 1 Mpc. This indicates that the Universe is very homogeneous at larger scales, but inhomogeneities might be present and common at smaller scales, as observed in surveys of the nearby Universe.

## ACKNOWLEDGMENTS

FJC and XB thank the DGICYT for financial support, under project PB92-00501. ACF thanks the Royal Society for support. FJC thanks E. Martínez-González for useful discussions. We thank G. Hasinger (the referee) and T. Miyaji for helpful comments and suggestions that improved the manuscript. We would like to thank the RIXOS consortium for letting us use the positions of their fields. This research has made use of data obtained from the Leicester Database and Archive Service at the Department of Physics and Astronomy, Leicester University, UK.

## REFERENCES

Almaini O., Shanks T., Boyle B. J., Griffiths R. E., Roche N., Stewart G. C., Georgentopoulos I., 1996, MNRAS, 282, 295
Barber C. R., Warwick R. S., 1994, MNRAS, 267, 270
Barcons X., 1992, ApJ, 396, 460
Barcons X., Branduardi-Raymont G., Warwick R. S., Fabian A. C., Mason K. O., McHardy I. M., Rowan-Robinson M., 1994, MNRAS, 268, 833
Barcons X., Fabian A. C., 1988, MNRAS, 230, 189
Bardeen J. M., Bond J. R., Kaiser N., Szalay A. S., 1986, ApJ, 304, 15
Bevington P. R., 1969, Data Reduction and Error Analysis for the Physical Sciences. McGraw-Hill, New York
Boyle B. J., Mo H. J., 1993, MNRAS, 260, 925
Boyle B. J., Shanks T., Georgantopoulos I., Stewart G. C., Griffiths R. E., 1994, MNRAS, 271, 639
Boyle B. J., McMahon R. G., Wilkes B. J., Elvis M., 1995, MNRAS, 272, 462
Branduardi-Raymont G. et al., 1994, MNRAS, 270, 947
Butcher J. A. et al., 1996, MNRAS, submitted
Carballo R., Warwick R. S., Barcons X., González-Serrano J. I., Barber C. R., Martínez-González E., Pérez-Fournon I., Burgos J., 1995, MNRAS, 277, 1312
Carrera F. J., Barcons X., Butcher J. A., Fabian A. C., Stewart G. C., Warwick R. S., Hayashida K., Kii T., 1991, MNRAS, 249, 698
Ciliegi P., Elvis M., Wilkes B. J., Boyle B. J., McMahon R. G., 1996, MNRAS, submitted
Efstathiou G., Bond J. R., White S. D. M., 1992, MNRAS, 258, 1P (EBW)
Gendreau K. C. et al., 1995, PASJ, 47, L5
Hasinger G., Turner T. J., George I. M., Boess G., 1992, NASA/GSFC OGIP Calibration Memo CAL/ROS/92-001
Hasinger G., Burg R., Giacconi R., Hartner G., Schmidt M., Trümper J., Zamorani G., 1993, A&A, 275, 1
Inoue H., Kii T., Ogasaka Y., Takahashi T., Ueda Y., 1996, in Zimmermann H. U., Trümper J., Yorke H., eds, Röntgenstrahlung from the Universe. MPE Report, 263, p. 323
Jones L. R. et al., 1995, in Maddox S., Aragón-Salamanca A., eds, Wide field spectroscopy and the distant Universe. World Scientific Press, Singapore, p. 346
Lampton M., Margon B., Bowyer S., 1976, ApJ, 208, 177
McCammon D., Sanders W. T., 1990, ARA&A, 28, 657
Miyaji T., 1994, PhD thesis, Univ. of Maryland
Mulchaey J. S., Davis D. S., Mushotzky R., Burstein D., 1996, ApJ, 456, 80
Olive K. A., Steigman G., 1995, ApJS, 97, 49
Page M. J. et al., 1996a, MNRAS, 281, 579
Page M. J., Mason K. O., McHardy I. M., Jones L. R., Carrera F. J., 1996b, MNRAS, submitted
Peebles P. J. E., 1980, the Large-Scale Structure of the Universe. Princeton Univ. Press, Princeton NJ
Peacock J. A., Dodds S. J., 1994, MNRAS, 267, 1020 (PD)
Piccinotti G., Mushotzky R. F., Boldt E. A., Holt S. S., Marshall F. E., Serlemitsos P. J., Shafer R. A., 1982, ApJ, 253, 485
Plucinsky P. P., Snowden S. L., Briel U. G., Hasinger G., Pfeffermann E., 1993, ApJ, 418, 519

Rees M. J., 1980, in Abell G. O., Peebles P. J. E., eds, Proc. IAU Symp. 92, Objects at High Redshift. Reidel, Dordrecht, p. 209
Romero-Colmenero E., Branduardi-Raymont G., Carrera F. J., Jones L. R., Mason K. O., McHardy I. M., Mittaz J. P. D., 1996, MNRAS, 282, 94
Rosati P., Della Ceca R., Burg R., Norman C., Giacconi R., 1995, ApJ, 445, L11
Scheuer P. A. G., 1974, MNRAS, 166, 329
Shanks T., Boyle B. J., 1994, MNRAS, 271, 753
Snowden S. L., Freyberg M. J., 1993, ApJ, 404, 403
Sołtan A. M., Hasinger G., 1994, A&A, 288, 77
Sołtan A. M., Hasinger G., Egger R., Snowden S., Trümper J., 1996, A&A, 305, 17
Vikhlinin A., Forman W., Jones C., Murray S., 1995, ApJ, 451, 564